Substrate-Independent Micropatterning of Polymer Brushes Based on Photolytic Deactivation of Chemical Vapor Deposition Based Surface-Initiated Atom-Transfer Radical Polymerization Initiator Films

Ramya Kumar,[†,‡] Alexander Welle,[§,∥] Fabian Becker,[§] Irina Kopyeva,[†,‡] and Joerg Lahann*[,†,§,‡]

[†]Department of Chemical Engineering and [‡]Biointerfaces Institute, University of Michigan, Ann Arbor, Michigan 48109, United States
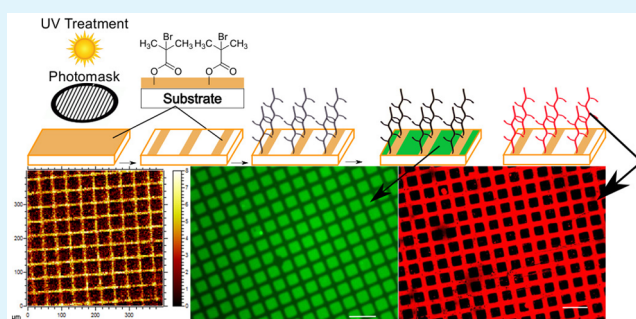
[§]Institute for Functional Interfaces (IFG) and [∥]Karlsruhe Nano Micro Facility, Karlsruhe Institute of Technology, Karlsruhe, Baden-Württemberg 76131, United States

S *Supporting Information*

ABSTRACT: Precise microscale arrangement of biomolecules and cells is essential for tissue engineering, microarray development, diagnostic sensors, and fundamental research in the biosciences. Biofunctional polymer brushes have attracted broad interest in these applications. However, patterning approaches to creating microstructured biointerfaces based on polymer brushes often involve tedious, expensive, and complicated procedures that are specifically designed for model substrates. We report a substrate-independent, facile, and scalable technique with which to prepare micropatterned biofunctional brushes with the ability to generate binary chemical patterns. Employing chemical vapor deposition

(CVD) polymerization, a functionalized polymer coating decorated with 2-bromoisobutyryl groups that act as atom-transfer radical polymerization (ATRP) initiators was prepared and subsequently modified using UV light. The exposure of 2-bromoisobutyryl groups to UV light with wavelengths between 187 and 254 nm resulted in selective debromination, effectively eliminating the initiation of ATRP. In addition, when coatings incorporating both 2-bromoisobutyryl and primary amine groups were irradiated with UV light, the amines retained their functionality after UV treatment and could be conjugated to activated esters, facilitating binary chemical patterns. In contrast, polymer brushes were selectively grown from areas protected from UV treatment, as confirmed by atomic force microscopy, time-of-flight secondary ion mass spectrometry, and imaging ellipsometry. Furthermore, spatial control over biomolecular adhesion was achieved in three ways: (1) patterned nonfouling brushes resulted in nonspecific protein adsorption to areas not covered with polymer brushes; (2) patterned brushes decorated with active binding sides gave rise to specific protein immobilization on areas presenting polymer brushes; (3) and primary amines were co-patterned along with clickable polymer brushes bearing pendant alkyne groups, leading to bifunctional reactivity. Because this novel technique is independent of the original substrate's physicochemical properties, it can be extended to technologically relevant substrates such as polystyrene, polydimethylsiloxane, polyvinyl chloride, and steel. With further work, the photolytic deactivation of CVD-based initiator coatings promises to advance the utility of patterned biofunctional polymer brushes across a spectrum of biomedical applications.

KEYWORDS: *micropatterned polymer brushes, protein patterning, chemical vapor deposition, SI-ATRP, biointerfaces*

1. INTRODUCTION

Several research areas in biomedical science require spatial control over the presentation of cells and biomolecules such as polysaccharides, growth factors, or extracellular matrix (ECM) proteins.[1] Examples of such research objectives include spatiotemporal control of interactions between cells and ECM proteins to elucidate signaling pathways,[2,3] high-throughput platforms for screening protein–protein and protein–glycan interactions for pharmacology and proteomic studies,[4] bioMEMS devices for diagnostics and sensing,[5]

engineering neuronal networks on synthetic materials[6] and well-defined protein arrays that direct stem cell fate using geometric and chemical cues.[7] Engineered biointerfaces are essential tools to accomplish these goals, and it is particularly desirable that platforms for obtaining custom biomolecular patterns are simple, substrate-independent, and scalable.

A rich toolbox of bottom-up and top-down surface engineering techniques has been developed to meet these challenges. Direct protein-writing approaches such as dip-pen nanolithography,[8] inkjet printing,[9] laser ablation, nanoimprint lithography[10] (NIL), polymer pen lithography[11] (PPL), colloidal lithography[12] (CL), and e-beam lithography[13] are geometrically versatile and allow for the orthogonal creation of multiplexed protein patterns. Unfortunately, these methods are often limited by low throughput and the requirement of multiple serial processing steps, each of which needs delicate handling, sometimes in cleanrooms.[14] Microcontact printing (μCP) and its variations have been widely used in creating protein arrays[15] and patterns[16] thanks to its inexpensive nature and flexibility of use in lab-on-chip and microfluidic applications.[17] However, μCP is a manual technique in which polydimethylsiloxane (PDMS) stamp collapse and issues associated with the stamp inking and drying processes can trigger operational errors.[18]

Alternatively, indirect approaches rely on patterned polymer brushes to direct biomolecular and cellular adhesion.[19] Polymer brushes have been used to impart the desired interfacial properties and create surfaces with tailored architectures or chemical and biological functionalities.[20] Depending on the brush composition, researchers have either engineered resistance to nonspecific protein adsorption[21] or precisely controlled the composition and orientation of proteins that can recognize and bind to bioactive polymer brushes through specific interactions.[16,22]
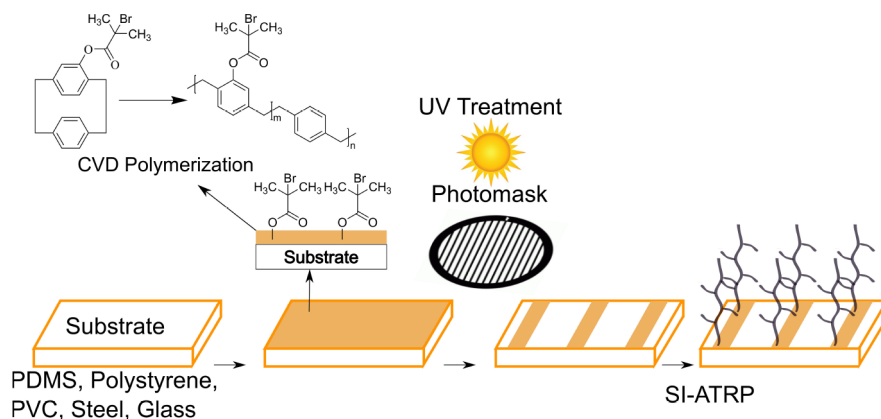
Polymer brush synthesis has benefited from the development of surface-initiated polymerization techniques such as surface-initiated atom-transfer radical polymerization (SI-ATRP),[23] surface-initiated radical addition−fragmentation transfer (SI-RAFT),[24] and surface-initiated nitroxide mediated polymerization (SI-NMP),[25] of which SI-ATRP is most widely used. Polymer brushes are typically synthesized in two steps: (i) immobilization of an SI-ATRP initiator (usually the bromoisobutyryl group) followed by (ii) SI-ATRP of the desired monomer from the initiation sites to form densely tethered polymer chains. By exerting spatial control over either of these two steps, it is possible to create micron and nanoscale patterns of polymer brushes.[26] The advent of oxygen-tolerant SI-RAFT[27] and SI-ATRP[28] has eliminated the necessity for specialized equipment (such as Schlenk lines and glove boxes) and formal training in air-free chemistry techniques, making polymer brushes more accessible to non-experts.[29] Previously developed polymer brush patterning strategies can be classified into four categories: (1) selective activation of a photosensitive iridium catalyst by irradiating the reaction system through a mask[30] or selective initiator functionalization via photolysis of nitrophenyl-protected molecules;[31] (2) creating patterns of the SI-ATRP initiator using DPN,[32−34] PPL,[11] or CL[35,36] techniques, μCP,[37] or the application of DOPA-based macroinitiators;[38−41] (3) post-polymerization top-down approaches involving selective degradation of the polymer brushes using e-beam treatment[42−44] or the use of photo-degradable polymer brushes;[45] (4) Spatially selective deactivation of the bromoisobutyryl initiator using near-UV photolithography[46−48] or by e-beam treatment.[49]

There are some shortcomings associated with current techniques for patterning polymer brushes. Photolabile monomers and photosensitive catalyst systems can be challenging to synthesize. Besides requiring clean room conditions, e-beam lithography is time-consuming when large

substrate areas and high numbers of substrates have to be patterned.[50] Common to all of these patterning approaches is that they are restricted to a limited number of specialized substrate choices, making it difficult to adapt them to "real" substrates employed in the life sciences, such as Petri dishes, well plates, microfluidic devices, or other plastics. Photolytic deactivation of silane-based initiator systems confine their application to Si/SiO$_2$ substrates, whereas μCP and DPN-based approaches rely on patterning gold substrates with thiol-based initiators. Specialized initiators have been developed for graphene,[51] graphene oxide,[52] polymers,[53,54] ITO,[55] and titanium[47] substrates, but they typically require extensive multistep synthesis. Overall, there is a need for a rapid, facile, and substrate-independent patterning strategy that resolves these technological issues while achieving a high degree of pattern fidelity and reproducibility.

Chemical vapor deposition (CVD) polymerization is a substrate-independent surface-modification tool that yields reactive coatings in a solvent-free, pinhole-free, and conformal manner.[56] Capable of forming robust and stable coatings on almost any substrate material,[8] CVD presents a versatile route to chemically reactive surfaces.[57] In the past, soft elastomeric stamps such as PDMS were used to transfer chemical patterns onto reactive CVD-based coatings via click reactions.[58,59] Subsequently, these patterns could be amplified into cellular and biomolecular patterns. CVD-mediated microstructuring was not limited to flat substrates; rather, three-dimensional objects were patterned by employing projection lithography on benzophenone-based CVD polymers.[60] Significantly, Jiang et al.[61] developed a CVD-based ATRP initiator immobilization strategy that decoupled SI-ATRP from the underlying surface chemistry. In addition to developing a bromoisobutyryl-based CVD precursor that could be vapor-deposited on any substrate, they employed vapor-assisted micropatterning in replica structures (VAMPIR)[62] to create patterned initiator surfaces. Due to its reliability, scalability, flexibility, and substrate independence, the combination of CVD with traditional patterning approaches has been highly beneficial. However, VAMPIR is typically limited to discontinuous patterns and intimate contact must be ensured between the PDMS construct and the substrate for VAMPIR to be effective.[63] Plasma-enhanced chemical vapor deposition (PE-CVD) has also enabled the substrate independent immobilization of ATRP initiators,[64−67] but it is unclear how patterned surfaces may be obtained from PE-CVD.

Here, we report a patterning strategy for polymer brushes using a CVD-based initiator coating that is substrate-independent and can promote the formation of polymer brushes along arbitrary micropatterns. Exposure of CVD-polymerized bromoisobutyryl coatings to UV light through a photomask deactivated the bromoisobutyryl groups while preserving the ATRP-initiating functionality of the masked regions.[46−48] This UV-treated surface was then employed as a substrate for SI-ATRP, resulting in well-defined patterns of polymer brushes. Our platform confers the ability to simultaneously process multiple patterns in parallel and can be applied to a large library of substrates as long as they are compatible with the CVD process, regardless of chemical composition and optical and mechanical properties. Moreover, the development of bioinert and bioactive polymer brushes makes it possible to orchestrate contrasting biointerfacial outcomes on these patterned brushes. Typically, in studies that employ photolytic initiator deactivation[46−48] to generate

Scheme 1. Spatioselective Deactivation of SI-ATRP Initiator Using UV-Ozone Treatment through a Photomask[a]

[a]Polymer brush growth only occurs from masked regions, whereas in treated regions, the initiator activity is suppressed.

patterned biofunctional polymer brushes, the UV-irradiated background would remain inert and nonfunctional, resulting in surfaces with limited chemical complexity. Recently, Madsen et al.[68] reported the formation of binary chemical patterns containing distinct cysteine and PEG domains using initiator deactivation. In contrast, we demonstrate binary chemical patterning by using CVD co-polymerization to co-pattern primary amine groups on UV-treated regions along with functional polymer brushes grown from masked regions.

2. RESULTS AND DISCUSSION

Scheme 1 outlines the first step, involving the coating of substrates with the SI-ATRP initiator, poly[(p-xylylene-4-methyl-2-bromoisobutyrate)-co-(p-xylylene)] (PPX-EB) through CVD polymerization of the precursor [2.2]-paracyclophane-4-methyl 2-bromoisobutyrate (PCP-EB). The thickness of these PPX-EB coatings was determined using ellipsometry and confirms the formation of the coating. Additionally, X-ray photoelectron spectroscopy (XPS) and Fourier transform infrared (FTIR) spectroscopy were performed to ascertain that the ATRP-initiating ester bromide functional groups were present (Figure S1a).

Next, PPX-EB-coated substrates were exposed through photomasks with hexagonal patterns to UV light for treatment times ranging from 10 to 20 min to understand the impact on the spatial distribution of residual bromine on the initiator layer. To measure bromine content as a function of spatial location (lateral and depth profiling), we employed time-of-flight secondary ion mass spectrometry (ToF-SIMS). Static ToF-SIMS has excellent surface sensitivity (<2 nm) and a lateral resolution of 150 nm and was hence employed to capture chemical contrasts across these patterns. To probe deeper layers and buried interfaces, dynamic SIMS based on erosion of the sample with an argon cluster ion beam was employed to capture chemical contrasts across these patterns. In Figure 1, the bromine distribution of the hexagonally patterned initiator coatings changes as a function of UV treatment time. We noticed that the highest intensity signals from the $^{79}Br^-$ and $^{81}Br^-$ fragments were emitted from the areas lying between the hexagons (yellowish in color), with the interiors of the hexagons displaying very low Br^- intensity (darker regions in the heatscale). An unexpected, albeit interesting observation was the progressive deterioration of pattern quality upon increasing UV treatment time. High-resolution images of the bromine chemical maps (Figure 1D−

F) revealed that the hexagonal borders, which bear bromine, become progressively narrower with increased treatment times. Also, characteristic halos could be discerned in the UV-treated regions inside the hexagons in the 15 and 20 min samples, signifying an increase in ablated area.

During UV treatment, deep UV light (between 185 and 257 nm) can generate ozone from oxygen.[69] The simultaneous action of UV light and ozone results in surface oxidation of carbon-based materials and is frequently employed for polymer surface modification and in stripping surfactant layers from end-capped Pt and Pd nanoparticles to improve their catalytic activity.[70] For SI-ATRP reactions to be initiated, the halogen atom (usually bromine) needs to be transferred from the initiator species to the coordination complex formed between the ligand and the Cu(I) bromide. If the bromine atom is absent on the initiator surface, SI-ATRP will not occur. Furthermore, ozone-triggered bromine depletion can explain why treatment time plays a critical role. Once the optimum treatment time is exceeded, UV-generated ozone diffuses under the mask and begins to eliminate bromine in areas covered by the mask. With a longer treatment time, the ozone diffuses across larger areas beneath the mask, explaining why we obtained differences in feature sizes despite using identical photomasks. These findings agree well with prior reports by Sheridan et al.[71] and Ahmad et al.,[48] who reported that UV treatment could deactivate the ATRP-initiating bromoisobutyryl groups and benzyl chloride groups, respectively.

To further our mechanistic understanding of the UV-induced bromine depletion process, we conducted XPS measurements of homogeneously treated PPX-EB surfaces (without photomasks) to understand how its elemental composition changes with UV treatment time. As seen in Figure 1G, the Br_{3d} signal at 70.3 eV can be clearly discerned from the untreated PPX-EB surface, whose theoretical bromine content is around 4.8%. However, after 30 min of UV treatment (Figure 1H), the peak intensity falls drastically and can no longer be discriminated from the background. Upon quantifying the area under the Br_{3d} peak obtained from high-resolution scans (Figure 1I), we observed that the bromine content was significantly reduced even within 5 min of UV exposure and continued to decrease steadily with increasing treatment time before being reduced to near-zero levels at 30 min. The quantification of high-resolution XPS spectra (Table S5) agreed well with our conclusions from the chemical maps generated by ToF-SIMS, where there were strong contrasts in
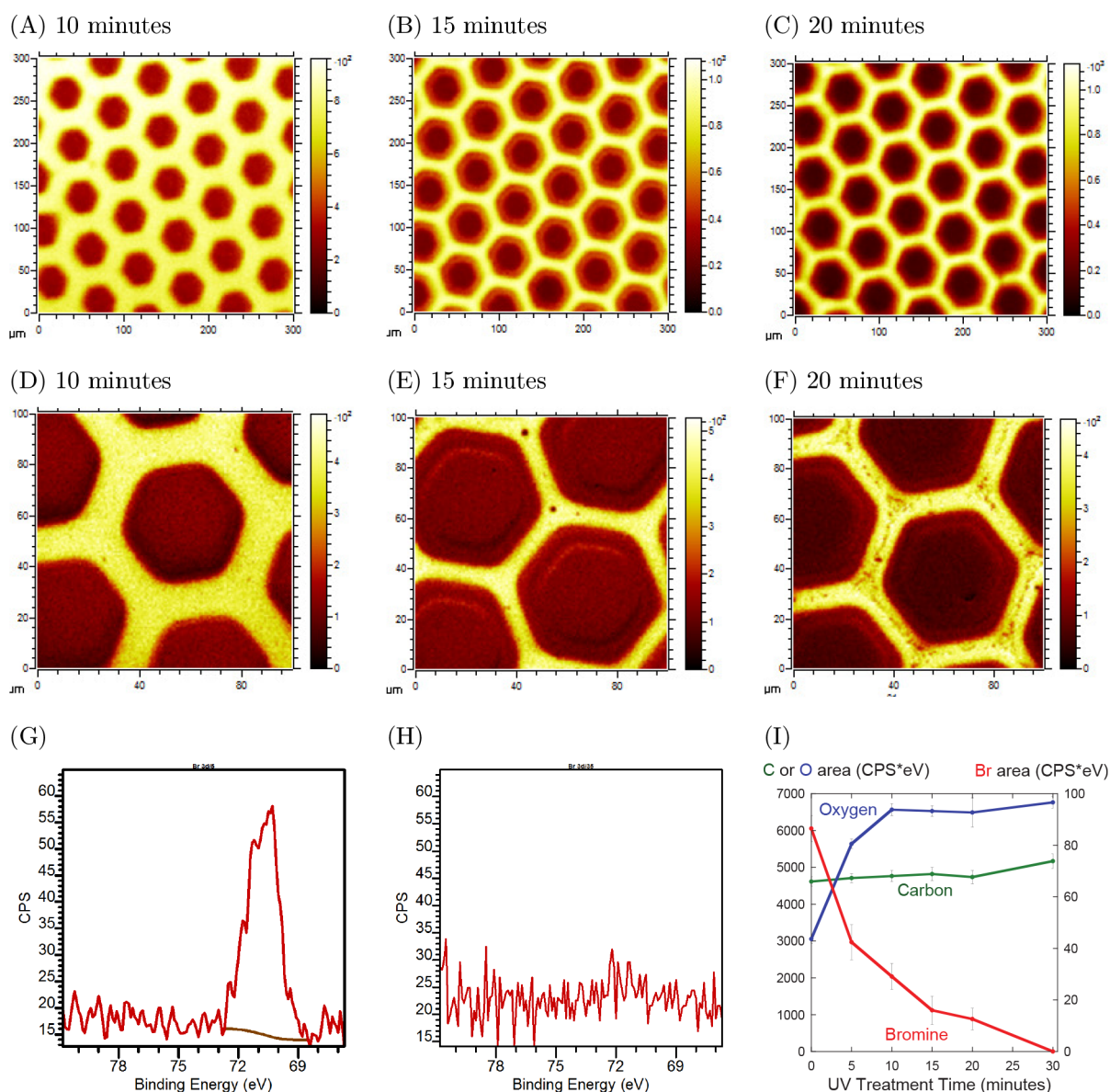
Figure 1. Evolution of vapor-deposited initiator (PPX-EB) surface composition with UV treatment. (A−F) Depth integrated lateral distribution of Br from ToF-SIMS (sum of both isotopes.) (A, D) Distribution of Br^- on PPX-EB surfaces treated for 10 min through a hexagonal photomask. (B, E) When treatment time was increased to 15 min, we could discern shrinkage in the areas previously emitting Br^-. This is apparent in the formation of a halo around the hexagonal borders and the reduced thickness of hexagon borders. (C, F) At the 20 min time point, we could observe a starker contrast between the interior of the hexagons and the borders. This was also accompanied by reduction of bromine content within the masked border regions, apparent in the red streaks formed in the yellow hexagonal bands. (G−I) XPS data of unpatterned samples. (G) High-resolution scan of Br_{3d} on PPX-EB prior to UV treatment. (H) High-resolution scan of Br_{3d} after 30 min of UV exposure. (I) Even 5 min of treatment causes a steep decrease in area under Br_{3d} peaks (red). This decrease continued with progressively higher UV treatment times until the peak disappeared. While the C_{1s} (green) area remained more or less constant with UV treatment, oxygen (blue) content increased significantly.

bromine content between treated and masked areas. Furthermore, we were able to glean additional insights from XPS, specifically the role of ozone in the initiator deactivation process. In contrast to Br_{3d}, the O_{1s} signal rises continually with UV exposure. The oxygen content was observed to increase from 18.3% for the untreated PPX-EB surfaces to 31.8% after 30 min of UV exposure. This indicates that the removal of bromine from the PPX-EB surface is accompanied by the transformation of C−H and C−Br bonds into aldehydes, alcohols, and acids by ozone. This conclusion is supported by the changes in the high-resolution C_{1s} spectra (Figure S5), which show a gradual increase in C=O and C−O signals with higher UV treatment times. Together, the XPS and ToF-SIMS

results suggest that the ability of PPX-EB to initiate polymer brush growth is hindered by its exposure to ozone.

Next, we proceeded to verify that the initiator patterns could be used to prepare microstructured polymer brushes. We grafted poly(2-methacryloyloxyethyl phosphorylcholine) (poly(MPC)) brushes from patterned PPX-EB substrates and acquired ToF-SIMS images, focusing on the PO_2^- and PO_3^- fragments emitted by the phosphorylcholine brushes. We observed a strong contrast in PO_2^- and PO_3^- signals owing to the high thickness and density of the poly(MPC) brushes in the masked areas compared with the dilute and short polymer chains present in the UV-treated regions. Regions from which PO_2^- and PO_3^- signals [characterizing the poly(MPC)
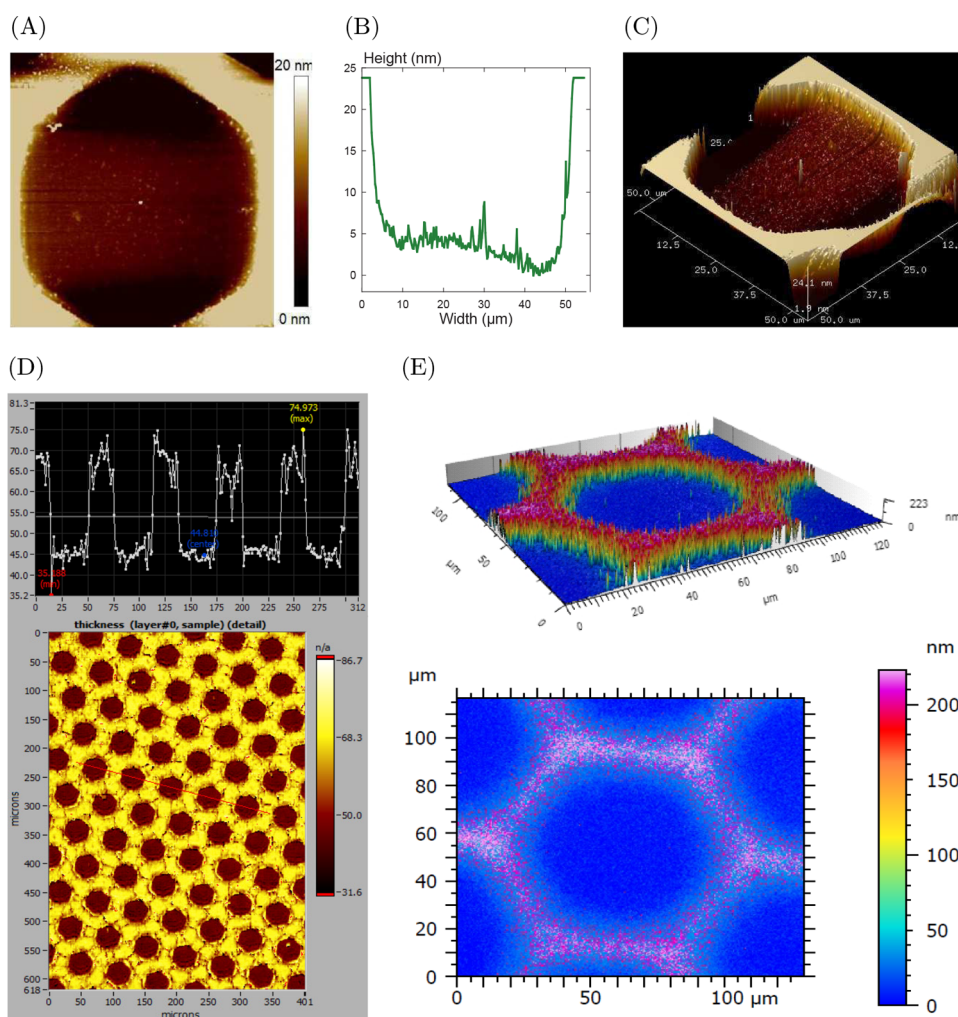
Figure 2. Atomic force microscopy (AFM) was used to visualize the topographic contrasts of patterned poly(MPC) brushes. (A) Two-dimensional topographical maps of the patterned poly(MPC) brushes obtained from AFM imaging of dry substrates. Topographic contrasts were congruent with the hexagonal geometry of the photomask employed. (B) Height profiles from AFM measurements. Brush heights of 20 nm were observed. (C) Three-dimensional projections of the patterned surfaces. (D) Imaging ellipsometry profiles indicate thickness differences of around 20−25 nm between UV-treated and untreated regions, consistent with the AFM results. Thick poly(MPC) brushes were formed only on untreated areas, whereas only a dilute thin layer resulted in the UV-treated areas. (E) Surface enhanced ellipsometric contrast (SEEC) measurements indicate that the poly(MPC) brushes present on the masked areas swell considerably, while the MPC oligomers present on the UV-treated areas do not swell.

brushes] were observed, overlapped with the areas from which the Br⁻ signals (associated with the initiator coatings) were recorded. The PO_x and bromide signals were co-localized in the masked areas, which were shielded from UV exposure (Figure S3), confirming that patterned polymer brushes arise from the patterned initiator coatings.

To demonstrate the geometric versatility and ease of controlling feature shapes, we prepared poly(MPC) brushes using initiator coatings patterned using photomasks with hexagonal (Figure 2), square and striped patterns (Figures S7 and S8). We characterized these patterned poly(MPC) brushes using atomic force microscopy (AFM) as shown in Figure 2A. In addition to the two-dimensional topographic map, the height profile (Figure 2B) and three-dimensional projection Figure 2C reveal thickness differences existing between the regions from which the brushes were successfully grafted and the irradiated regions. We observed that the hexagonal geometry of the brushes conformed to that of that of the patterned photomask employed. Using AFM, we also confirmed that the dry brush thickness was between 20 and

25 nm. To complement the AFM study, brush thickness was studied as a function of spatial location using imaging ellipsometry. From Figure 2D, we discerned the variation in brush thickness between areas where the polymer brush growth was allowed to proceed and the areas where brush growth was inhibited. While imaging ellipsometry provides estimates of thickness differences between the brush-bearing regions and the surrounding brush-free substrate, it must be noted that it is not suitable to assess the absolute values of thickness. Thickness differences from imaging ellipsometry were found to be around 25 nm, which agrees well with the differences in dry thickness reported by the AFM study. Finally, we assessed the swelling behavior of these patterned brushes using surface-enhanced ellipsometric contrast[72] (SEEC) measurements (Figure 2E). Upon placing the substrates in a 10 mM phosphate-buffered solution (PBS), we were able to obtain an approximate estimate of the differences in swollen thickness between the dense thick brushes on the masked areas and the dilute short chains formed on the irradiated areas. In the dry state, we had
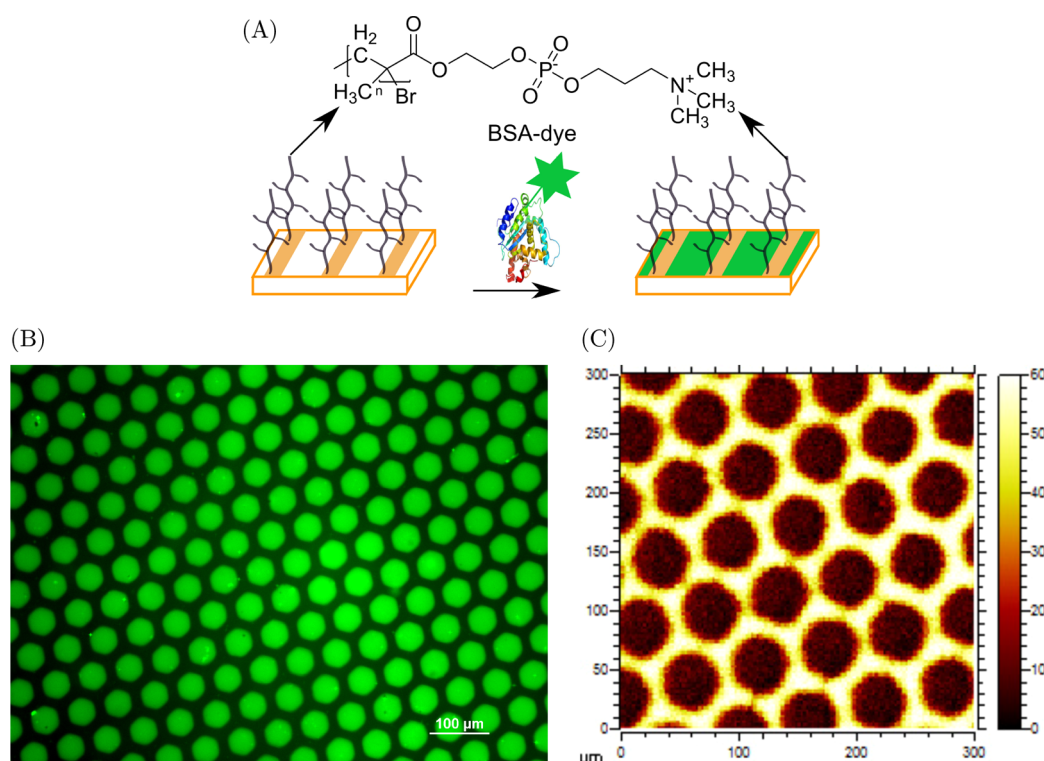
Figure 3. (A) Controlled deposition of fluorescent BSA occurs in areas where zwitterionic poly(2-methacryloyloxyethyl phosphorylcholine) (poly(MPC)) brushes are absent. No protein adhesion occurs in domains where the poly(MPC) brushes are grafted. (B) Fluorescence-labeled bovine serum albumin only adheres to regions where poly(MPC) is absent. Scale bar is 100 μm. (C) ToF-SIMS snapshot of PO_2^- and PO_3^- fragments reveal high phosphonate intensity in untreated areas but very weak signals from treated areas. The co-localization of BSA deposition and areas of low phosphonate intensity suggests that our patterning strategy was successful.

observed a thickness difference of 25 nm between the UV-treated initiator background and the brushes grafted from masked areas. After 10 min of equilibration with PBS, this thickness difference increased 8-fold to nearly 200 nm, indicating that the poly(MPC) brushes were considerably swollen. In contrast, the oligomers present on the irradiated areas did not appear to swell. It has been reported that brush swelling is not only dependent on the solvent quality but also on the grafting density, with high-density and medium-density brushes exhibiting a high swelling response, unlike low-density polymer chains.[73] From the SEEC images, swelling could not be detected from the residual MPC oligomers originating from the bromine-depleted regions, unlike the high degree of swelling observed from the poly(MPC) brushes grafted from the intact initiator regions. Our SEEC study affirms that functional polymer brushes with high density and thickness cannot be grafted from the initiator molecules treated with UV.

We further hypothesized that the exceptional resistance of poly(MPC) brushes to nonspecific protein adsorption[74] should lead to the selective deposition of proteins such as bovine serum albumin on domains where the initiator was deactivated and where poly(MPC) brush growth was prevented. We thus challenged these surfaces with a solution of BSA labeled with a fluorescent molecule and imaged the substrate thereafter (Figure 3). In Figure 3B, it is evident that bovine serum albumin (BSA) adhesion only happened in areas where the brushes were absent and that no protein adsorption occurred in areas where the brushes were grafted. To substantiate this conclusion, these substrates were characterized in parallel using ToF-SIMS (Figure 3C). We observed that the PO_2^- and PO_3^- signals associated with the poly(MPC) brushes emanated from

the same regions where protein adhesion was circumvented. This unambiguously establishes that a high level of geometric control over nonspecific protein deposition was achieved by controlling the spatial distribution of nonfouling brushes. If we consider the results gathered from complementary studies involving AFM, imaging ellipsometry, SEEC, ToF-SIMS, and BSA adsorption, we can conclude that our approach to polymer brush patterning represents a viable and robust path to creating protein patterns.

Next, we designed biointerfaces with specific interactions between biomolecules and polymer brushes. We engineered patterned polymer brushes presenting reactive alkyne side chains that can be further functionalized with biomolecules via click chemistry. To this end, we prepared copolymer brushes composed of propargyl methacrylate[75] and zwitterionic monomer, [2-(methacryloyloxy)ethyl]dimethyl-(3-sulfopropyl)ammonium hydroxide (MEDSAH) from patterned initiator surfaces (Figure 4). These copolymer brushes are designed such that the hydrophilic MEDSAH ensures that that nonspecific protein adhesion is prevented,[76] while the propargyl methacrylate offers reactive groups to which biomolecules such as biotin can be tethered via Husigen's copper-catalyzed 1,3-alkyne azide cycloaddition (CuAAC).[58] Using FTIR spectroscopy (Figure 4B), we verified that the pendant alkyne groups (at 3300 and 2125 cm^{-1}) as well as the sulfobetaine side chains were present in the copolymer brushes. Moreover, the ratio between the propargyl methacrylate and MEDSAH repeat units can be varied by modifying the composition of the monomer feed as seen in Figure 4C. Next, biotin−PEG−azide was clicked to the alkyne side chains in the patterned copolymer brushes using copper(I)-catalyzed
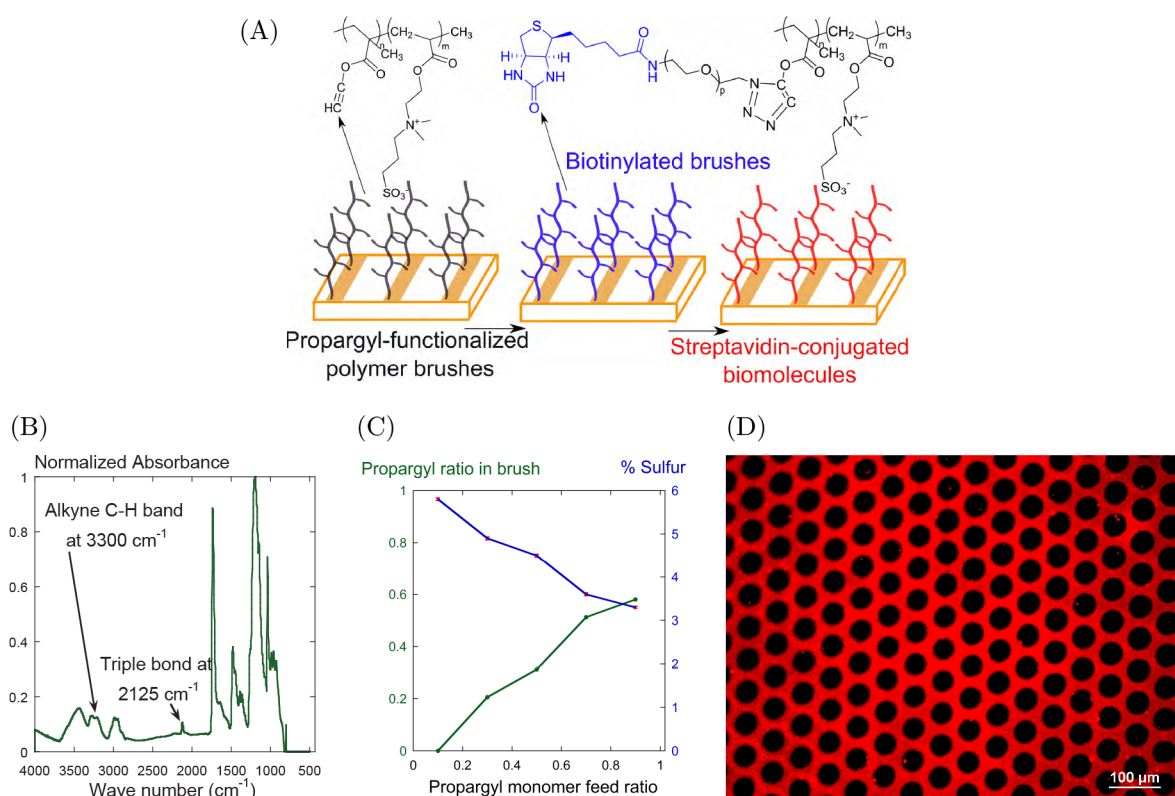
Figure 4. Generic strategy for engineering specific interactions between proteins and microstructured polymer brushes. (A) In the first step, copolymer brushes, poly(propargyl methacrylate-*co*-{[2-(methacryloyloxy) ethyl] dimethyl-(3-sulfopropyl) ammonium hydroxide}), consisting of zwitterionic repeat units and clickable alkyne-containing repeat units were grafted from the patterned initiator layer. Then, biotin-PEG-azide was clicked to the reactive alkyne side chains in the brushes. Finally streptavidin-conjugated molecules were immobilized to the patterned polymer brushes by taking advantage of the strong and specific interaction between streptavidin and biotin. (B) FTIR confirms the presence of alkyne groups in the copolymer brushes, which were then conjugated to biotin-PEG-azide molecules. (C) XPS measurements of sulfur content indicate that the ratio of propargyl repeat units and thereby the degree of biotinylation can be tuned by varying the monomer feed composition. (D) Biotinylated brushes bound to streptavidin bearing a fluorescent tag. This approach can be generalized to precisely pattern any streptavidin-conjugated biomolecule. Scale bar: 100 μm.
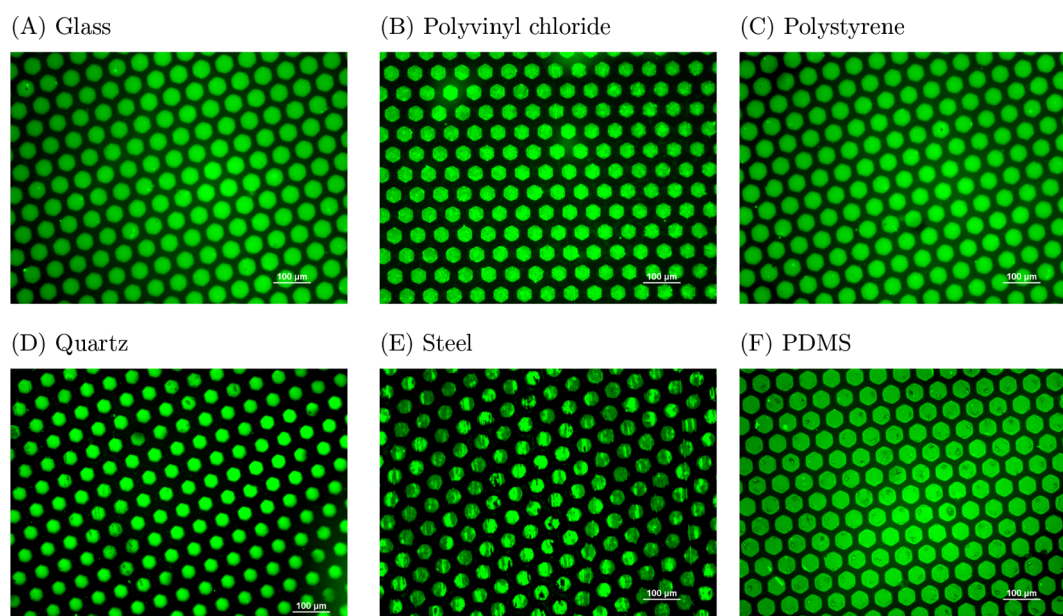

Figure 5. Our patterning approach can be applied to virtually any substrate, independent of surface chemistry. Fluorescence micrographs of BSA bound to patterned poly(MPC) brushes grown from initiator (PPX-EB) coatings that were vapor deposited on (A) glass, (B) polyvinyl chloride, (C) polystyrene, (D) quartz, (E) steel, and (F) polydimethylsiloxane (PDMS). These images demonstrate that patterning quality can be obtained not only on a model substrate but also on conventional polymers and metals. Scale bar: 100 μm.
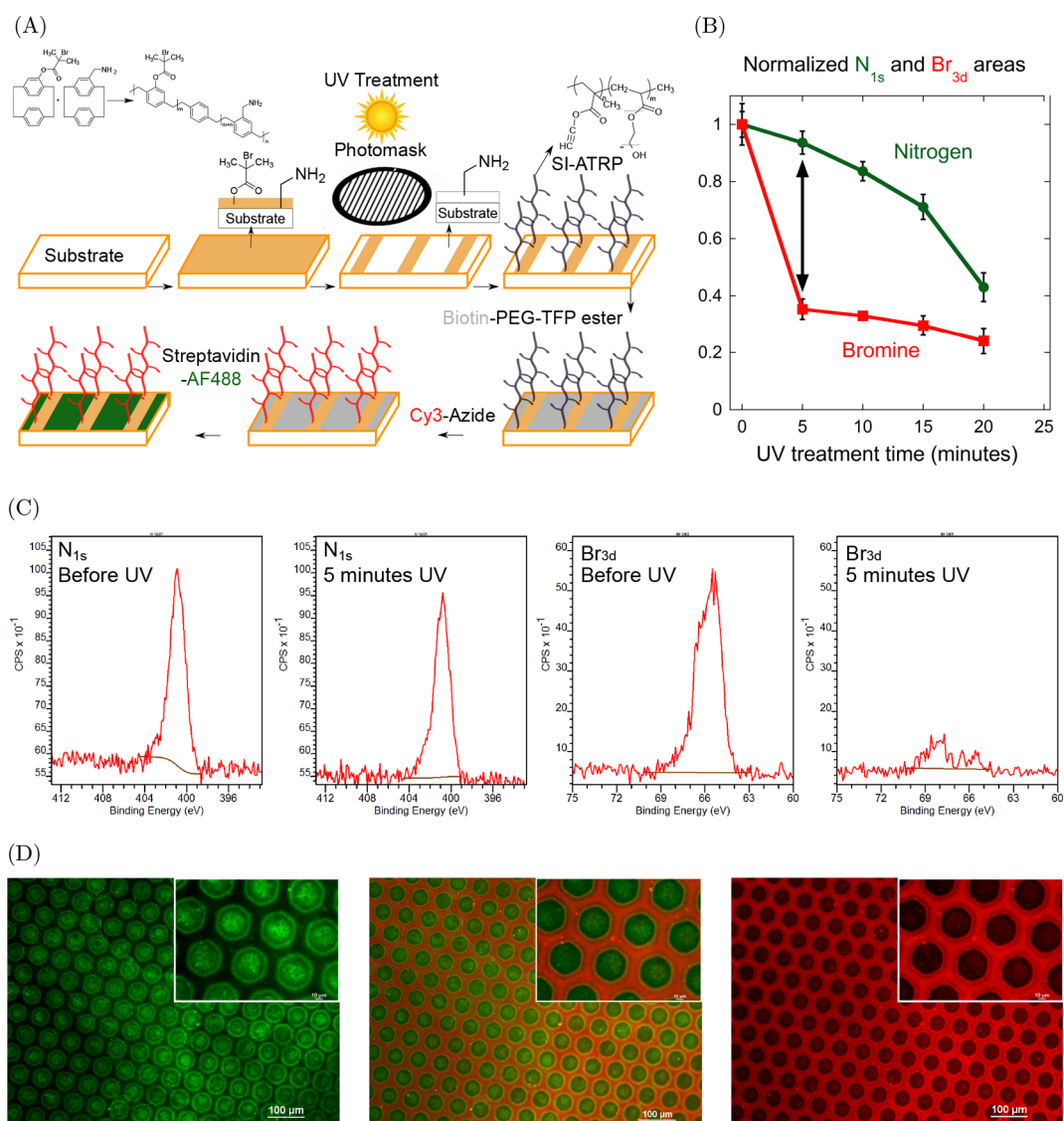
Figure 6. (A)Poly[(*p*-xylylene-4-methyl-2-bromoisobutyrate)-*co*-(*p*-xylylene-4-aminomethyl)-*co*-(*p*-xylylene)] or PPX-AM/EB were synthesized via CVD co-polymerization and then selectively debrominated using UV treatment. While the composition of the masked regions of the coating remain unaffected, UV-treated areas are selectively depleted of bromine while still retaining primary amine groups. (B, C) XPS quantification of nitrogen and bromine content as a function of UV treatment time. While the area of the Br_{3d} peak decreases steeply within 5 min of UV treatment, only a slight decrease in the area of N_{1s} was noticed. (D) Fluorescence microscopy was used to confirm successful azide−alkyne cycloaddition occurring along the polymer brushes (red) and the surface conjugation of TFP−ester with the primary amine groups on the treated areas (green). Scale bar: 100 μm.

alkyne−azide cycloaddition (CuAAC). Subsequently, we exploited the strong and specific affinity existing between streptavidin and biotin to immobilize streptavidin-cy3 onto the biotinylated brushes. Ultimately, we obtained streptavidin-cy3 patterns in the form of fluorescent hexagons (Figure 4D), consistent with the dimensions of the photomask. By engineering specific interactions between patterned polymer brushes and proteins, we were able to develop and validate a simple protein-patterning approach that can be employed generically for patterning any streptavidin-conjugated biomolecule.

To demonstrate the substrate independence of our technique, we created protein patterns based on nonspecific BSA adhesion around microstructured poly(MPC) brushes grafted from diverse substrates. Apart from the model substrates glass and quartz, we also studied patterned brush

formation on poly(vinyl chloride) (PVC), polystyrene (PS), polydimethylsiloxane, and steel (Figure 5). Although these substrates vary widely in their mechanical, optical, and interfacial properties (roughness, refractive index, hardness, surface charge, and hydrophobicity), comparable pattern quality was obtained on all substrates, including the steel substrates, which possessed micron-scale surface roughness. Our technique can therefore be applied not only for model surfaces such as gold, silicon, and glass but also for technologically more-relevant "non-model" materials possessing less-than-ideal surface characteristics.

With the objective of enhancing the functionality of our patterned surfaces, we turned to CVD co-polymerization to synthesize a copolymer coating, poly[(*p*-xylylene-4-methyl-2-bromoisobutyrate)-*co*-(*p*-xylylene-4-aminomethyl)-*co*-(*p*-xyly-lene)], abbreviated as PPX-AM/EB. As seen in the schematic

in Figure 6, the CVD copolymer possesses orthogonal reactivity via either CH_2NH_2 (AM) or bromoisobutyryl (EB) groups. We hypothesized that while UV treatment would result in the cleavage of the weak and labile C−Br bonds and subsequent bromine depletion, the C−N bonds in the AM groups would remain intact, preserving the reactivity of the primary amines (Figure 6A). To verify this conjecture, we collected high-resolution scans of the N_{1s} and Br_{3d} regions characteristic of AM and EB for PPX-AM/EB coatings treated with UV light for different durations (0−20 min). In Figure 6B, we can observe the evolution of areas (normalized to their initial pretreatment values) under the N_{1s} and Br_{3d} signals as a function of treatment time. While the Br_{3d} area drops precipitously within 5 min and then continues to decrease slowly before attaining a plateau, the opposite trend was observed with N_{1s}. For N_{1s}, the decrease in area was insignificant at short treatment times (5 and 10 min) and significant losses were observed only from the 15 min time point onward. It appears that these differences the kinetics of C−Br and C−N cleavage can be exploited by careful optimization of UV treatment time. By limiting the UV treatment time to 5 min, the PPX-AM/EB surface can be substantially debrominated while yet retaining the AM groups (Figure 6C).

Accordingly, we treated PPX-AM/EB surfaces with UV light for 5 min through a photomask, delineating the coating into UV-treated regions populated with AM groups and masked regions in which both AM and EB groups are present in their original surface concentrations. From these patterned PPX-AM/EB surfaces, we proceeded to graft poly[(propargyl methacrylate)-co-(oligo{ethylene glycol} methyl ether methacrylate)] or poly(PMA-co-OEGMA) brushes through SI-ATRP. Subsequently, we immobilized two fluorescent dyes onto the surface, a Cy-3 azide, which reacts exclusively with the patterned poly(PMA-co-OEGMA) brushes through the CuAAC reaction. The primary amines in the UV-treated areas underwent an orthogonal reaction with biotin-PEG-TFP ester molecules, which carry tetrafluorophenyl (TFP) esters, capable of forming amide bonds with primary amine groups. To these biotinylated amine groups, streptavidin-AF488 dye was bound as the final step of the surface immobilization protocol depicted in Figure 6A. It is pertinent to note that while primary amine groups are present both in the UV-treated regions that lack polymer brushes and also at the base of the 40 nm thick polymer brushes grafted from masked areas, amines in the latter are hindered from participating in the reaction with the activated esters due to the steric barrier imposed by the poly(PMA-co-OEGMA) brushes. As a result, the fluorescence resulting from the amide formation is restricted to the UV-treated areas as shown in the green channel of Figure 4D. Similarly, the Cy3 azide reacts exclusively with the pendant alkynes on the polymer brushes, as seen in the red channel of Figure 4D. The overlay suggests that, except for the inner borders of the hexagon (which appear yellow due to co-localization of both dyes), each reaction was restricted to its target regions. We suspect that the polymer brush conformation at the edges of the inner borders is not fully extended and is therefore unable to block the amines from the approaching activated ester. Overall, we conclude that our bifunctional surfaces composed of primary amines and alkyne-bearing polymer brushes can be employed to copattern two biomolecules along discretely defined regions, allowing for binary chemical and biomolecular patterns.

3. CONCLUSIONS

In summary, we have developed and validated a facile and substrate-independent approach to patterning proteins through specific and nonspecific means using microstructured polymer brushes. Our patterning strategy relies on spatially selective deactivation of vapor-deposited SI-ATRP initiator coatings by combining a patterned photomask with UV treatment. Mechanistically, we demonstrate that the ozone formed under these conditions plays a critical role in the deactivation of the ATRP initiator groups. After SI-ATRP, AFM, swelling studies, and imaging ellipsometry revealed thickness and topographical contrasts between the polymer brush domains and the inactivated regions. Chemical characterization of the patterned brushes was completed using ToF-SIMS, which substantiated the conclusions from AFM, swelling experiments, and ellipsometry. Further, we demonstrated patterned non-fouling brushes that spatially regulate nonspecific protein adsorption as well as biotinylated brushes that promote specific protein recognition events on the desired locations. Finally, by combining CVD co-polymerization with UV treatment, primary amine groups can be incorporated within UV-treated areas, enabling binary patterns. Using these bifunctional surfaces, we demonstrated that activated ester moieties can be co-patterned along with reactive polymer brushes, resulting in higher degrees of functionality and complexity. Given the prominent utility of polymer brushes in biotechnology,[19] this surface-modification approach will likely find broad applicability in cell patterning, high-throughput screening, bioMEMS devices, and enzymatic assays.

4. EXPERIMENTAL SECTION

Chemical vapor deposition polymerization procedures for synthesizing PPX-EB and PPX-AM/EB are described in Jiang et al.[61] and in the Supporting Information. Patterning was performed using UVJ144AX (Jet Light, CA) and copper TEM grids as photomasks (Structure Probe Inc.). Polymer brushes were grafted from patterned initiator surfaces using typical air-free SI-ATRP techniques described in the Supporting Information. Dimension Icon (Bruker, WI) was the AFM instrument used to obtain topographical information in the tapping mode. Imaging ellipsometry was performed using EP3 nanofilm (Accurion GmbH) on silicon and gold substrates. Nikon E-800 was used to collect fluorescence micrographs, and all fluorescent proteins were purchased from Thermo Fisher, Lumiprobe Inc., and Sigma-Aldrich. A ToF SIMS5 (ION-TOF GmbH, Munster, Germany) was used for collecting elemental maps of the surfaces. High-resolution XPS was performed using Krato Axis Ultra with a pass energy of 20 eV. Polymeric substrates were purchased from Ted Pella Inc. (Redding, CA) and metallic substrates from Goodfellow Inc. (Huntingdon, UK). SEEC measurements were performed on the N-Lab Station (Nanolane)

■ ASSOCIATED CONTENT

Ⓢ Supporting Information

The Supporting Information is available free of charge on the ACS Publications website at DOI: 10.1021/acsami.8b11525.

> FTIR spectra, ellipsometry data, additional ToF-SIMS maps, additional micrographs, XPS spectra, and experimental details (PDF)
>
> Video showing a 3D representation of ToF-SIMS data (AVI)
>
> Video showing a 3D representation of ToF-SIMS data (AVI)

■ AUTHOR INFORMATION

Corresponding Author

*E-mail: lahann@umich.edu.

ORCID Ⓐ

Ramya Kumar: 0000-0002-8725-0023

Notes

The authors declare no competing financial interest.

■ ACKNOWLEDGMENTS

■ REFERENCES

(1) Lee, K.-B.; Park, S.-J.; Mirkin, C. A.; Smith, J. C.; Mrksich, M. Protein Nanoarrays Generated By Dip-Pen Nanolithography. *Science* **2002**, *295*, 1702−1705.

(2) Falconnet, D.; Csucs, G.; Grandin, H. M.; Textor, M. Surface Engineering Approaches to Micropattern Surfaces for Cell-based Assays. *Biomaterials* **2006**, *27*, 3044−3063.

(3) Tseng, P.; Di Carlo, D. Substrates with Patterned Extracellular Matrix and Subcellular Stiffness Gradients Reveal Local Biomechanical Responses. *Adv. Mater.* **2014**, *26*, 1242−1247.

(4) Oyelaran, O.; Gildersleeve, J. C. Glycan Arrays: Recent Advances and Future Challenges. *Curr. Opin. Chem. Biol.* **2009**, *13*, 406−413.

(5) Hushegyi, A.; Pihikova, D.; Bertok, T.; Adam, V.; Kizek, R.; Tkac, J. Ultrasensitive Detection of Influenza Viruses with a Glycan-based Impedimetric Biosensor. *Biosens. Bioelectron.* **2016**, *79*, 644−649.

(6) Offenhausser, A.; Bocker-Meffert, S.; Decker, T.; Helpenstein, R.; Gasteier, P.; Groll, J.; Moller, M.; Reska, A.; Schafer, S.; Schulte, P.; Vogt-Eisele, A. Microcontact Printing of Proteins for Neuronal Cell Guidance. *Soft Matter* **2007**, *3*, 290−298.

(7) Tan, K. Y.; Lin, H.; Ramstedt, M.; Watt, F. M.; Huck, W. T. S.; Gautrot, J. E. Decoupling Geometrical and Chemical Cues Directing Epidermal Stem Cell Fate on Polymer Brush-based Cell Micropatterns. *Integr. Biol.* **2013**, *5*, 899−910.

(8) Chen, H. Y.; Hirtz, M.; Deng, X.; Laue, T.; Fuchs, H.; Lahann, J. Substrate-independent Dip-pen Nanolithography Based on Reactive Coatings. *J. Am. Chem. Soc.* **2010**, *132*, 18023−18025.

(9) Delaney, J. T.; Smith, P. J.; Schubert, U. S. Inkjet Printing of Proteins. *Soft Matter* **2009**, *5*, 4866−4877.

(10) Hoff, J. D.; Cheng, L. J.; Meyhöfer, E.; Guo, L. J.; Hunt, A. J. Nanoscale Protein Patterning by Imprint Lithography. *Nano Lett.* **2004**, *4*, 853−857.

(11) Xie, Z.; Chen, C.; Zhou, X.; Gao, T.; Liu, D.; Miao, Q.; Zheng, Z. Massively Parallel Patterning of Complex 2D and 3D Functional Polymer Brushes by Polymer pen Lithography. *ACS Appl. Mater. Interfaces* **2014**, *6*, 11955−11964.

(12) Wood, M. Colloidal Lithography and Current Fabrication Techniques Producing In-plane Nanotopography for Biological Applications. *J. R. Soc., Interface* **2007**, *4*, 1−17.

(13) Bat, E.; Lee, J.; Lau, U. Y.; Maynard, H. D. Trehalose Glycopolymer Resists Allow Direct Writing of Protein Patterns by Electron-beam Lithography. *Nat. Commun.* **2015**, *6*, 6654.

(14) Javaherian, S.; O'Donnell, K. A.; McGuigan, A. P. A Fast and Accessible Methodology for Micro-Patterning Cells on Standard Culture Substrates Using Parafilm Inserts. *PLoS One* **2011**, *6*, 1−8.

(15) Suh, K.; Langer, R.; Lahann, J. A Novel Photodefinable Reactive Polymer Coating and Its Use for Microfabrication of Hydrogel Elements. *Adv. Mater.* **2004**, *16*, 1401−1405.

(16) Gautrot, J. E.; Huck, W. T. S.; Welch, M.; Ramstedt, M. Protein-resistant NTA-functionalized Polymer Brushes for Selective and Stable Immobilization of Histidine-tagged Proteins. *ACS Appl. Mater. Interfaces* **2010**, *2*, 193−202.

(17) Voskuhl, J.; Brinkmann, J.; Jonkheijm, P. Advances in Contact Printing Technologies of Carbohydrate, Peptide and Protein arrays. *Curr. Opin. Chem. Biol.* **2014**, *18*, 1−7.

(18) Filipponi, L.; Livingston, P.; Kašpar, O.; Tokárová, V.; Nicolau, D. V. Protein Patterning by Microcontact Printing Using Pyramidal PDMS Stamps. *Biomed. Microdevices* **2016**, *18*, 1−7.

(19) Krishnamoorthy, M.; Hakobyan, S.; Ramstedt, M.; Gautrot, J. E. Surface-Initiated Polymer Brushes in the Biomedical Field: Applications in Membrane Science, Biosensing, Cell Culture, Regenerative Medicine and Antibacterial Coatings. *Chem. Rev.* **2014**, *114*, 10976−11026.

(20) Chen, T.; Amin, I.; Jordan, R. Patterned Polymer Brushes. *Chem. Soc. Rev.* **2012**, *41*, 3280.

(21) Bernards, M. T.; Cheng, G.; Zhang, Z.; Chen, S.; Jiang, S. Nonfouling Polymer Brushes via Surface-Initiated, Two-Component Atom Transfer Radical Polymerization. *Macromolecules* **2008**, *41*, 4216−4219.

(22) Waichman, S.; Bhagawati, M.; Podoplelova, Y.; Reichel, A.; Brunk, A.; Paterok, D.; Piehler, J. Functional Immobilization and Patterning of Proteins by an Enzymatic Transfer Reaction. *Anal. Chem.* **2010**, *82*, 1478−1485.

(23) Pyun, J.; Kowalewski, T.; Matyjaszewski, K. Synthesis of Polymer Brushes Using Atom Transfer Radical Polymerization. *Macromol. Rapid Commun.* **2003**, *24*, 1043−1059.

(24) Barbey, R.; Lavanant, L.; Paripovic, D.; Schüwer, N.; Sugnaux, C.; Tugulu, S.; Klok, H.-A. Polymer brushes Via Surface-initiated Controlled Radical Polymerization: Synthesis, Characterization, Properties, and Applications. *Chem. Rev.* **2009**, *109*, 5437−527.

(25) Hawker, C. J.; Bosman, A. W.; Harth, E. New Polymer Synthesis by Nitroxide Mediated Living Radical Polymerizations. *Chem. Rev.* **2001**, *101*, 3661−3688.

(26) Zoppe, J. O.; Ataman, N. C.; Mocny, P.; Wang, J.; Moraes, J.; Klok, H. A. Surface-Initiated Controlled Radical Polymerization: State-of-the-Art, Opportunities, and Challenges in Surface and Interface Engineering with Polymer Brushes. *Chem. Rev.* **2017**, *117*, 1105−1318.

(27) Shanmugam, S.; Xu, J.; Boyer, C. Aqueous RAFT Photopolymerization with Oxygen Tolerance. *Macromolecules* **2016**, *49*, 9345−9357.

(28) Yang, Q.; Lalevée, J.; Poly, J. Development of a Robust Photocatalyzed ATRP Mechanism Exhibiting Good Tolerance to Oxygen and Inhibitors. *Macromolecules* **2016**, *49*, 7653−7666.

(29) Discekici, E. H.; Pester, C. W.; Treat, N. J.; Lawrence, J.; Mattson, K. M.; Narupai, B.; Toumayan, E. P.; Luo, Y.; McGrath, A. J.; Clark, P. G.; Read de Alaniz, J.; Hawker, C. J. Simple Benchtop Approach to Polymer Brush Nanostructures Using Visible-Light-Mediated Metal-Free Atom Transfer Radical Polymerization. *ACS Macro Lett.* **2016**, *5*, 258−262.

(30) Page, Z. A.; Narupai, B.; Pester, C. W.; Bou Zerdan, R.; Sokolov, A.; Laitar, D. S.; Mukhopadhyay, S.; Sprague, S.; McGrath, A. J.; Kramer, J. W.; Trefonas, P.; Hawker, C. J. Novel Strategy for Photopatterning Emissive Polymer Brushes for Organic Light Emitting Diode Applications. *ACS Cent. Sci.* **2017**, *3*, 654−661.

(31) Johnson, A.; Madsen, J.; Chapman, P.; Alswieleh, A.; Al Jaf, O.; Bao, P.; Hurley, C.; Cartron, M. L.; Evans, S.; Hobbs, J.; Hunter, N.; Armes, S. P.; Leggett, G. J. Micrometre and Nanometre Scale Patterning of Binary Polymer Brushes, Supported Lipid Bilayers and Proteins. *Chem. Sci.* **2017**, *8*, 4517−4526.

(32) Zhou, X.; Wang, X.; Shen, Y.; Xie, Z.; Zheng, Z. Fabrication of Arbitrary Three-dimensional Polymer Structures by Rational Control of the Spacing Between Nanobrushes. *Angew. Chem., Int. Ed.* **2011**, *50*, 6506−6510.

(33) Zhou, X.; Liu, X.; Xie, Z.; Zheng, Z. 3D-patterned Polymer Brush Surfaces. *Nanoscale* **2011**, *3*, 4929−4939.

(34) Chen, C.; Zhou, X.; Xie, Z.; Gao, T.; Zheng, Z. Construction of 3D Polymer Brushes by Dip-pen Nanodisplacement Lithography: Understanding the Molecular Displacement for Ultrafine and High-speedPatterning. *Small* **2015**, *11*, 613−621.

(35) Li, Y.; Zhang, J.; Fang, L.; Jiang, L.; Liu, W.; Wang, T.; Cui, L.; Sun, H.; Yang, B. Polymer Brush Nanopatterns with Controllable Features for Protein Pattern Applications. *J. Mater. Chem.* **2012**, *22*, 25116.

(36) Li, Y.; Zhang, J.; Liu, W.; Li, D.; Fang, L.; Sun, H.; Yang, B. Hierarchical Polymer Brush Nanoarrays: A Versatile Way to Prepare Multiscale Patterns of Proteins. *ACS Appl. Mater. Interfaces* **2013**, *5*, 2126−2132.

(37) Kettling, F.; Vonhören, B.; Krings, J. A.; Saito, S.; Ravoo, B. J. One-step Synthesis of Patterned Polymer Brushes by Photocatalytic Microcontact Printing. *Chem. Commun.* **2015**, *51*, 1027−1030.

(38) Fan, X.; Lin, L.; Dalsin, J. L.; Messersmith, P. B. Biomimetic Anchor for Surface-initiated Polymerization from Metal Substrates. *J. Am. Chem. Soc.* **2005**, *127*, 15843−15847.

(39) Wei, Q.; Yu, B.; Wang, X.; Zhou, F. Stratified Polymer Brushes from Microcontact Printing of Polydopamine Initiator on Polymer Brush Surfaces. *Macromol. Rapid Commun.* **2014**, *35*, 1046−1054.

(40) Rodriguez-Emmenegger, C.; Preuss, C. M.; Yameen, B.; Pop-Georgievski, O.; Bachmann, M.; Mueller, J. O.; Bruns, M.; Goldmann, A. S.; Bastmeyer, M.; Barner-Kowollik, C. Controlled Cell Adhesion on Poly(dopamine) Interfaces Photopatterned with Non-fouling Brushes. *Adv. Mater.* **2013**, *25*, 6123−6127.

(41) Edmondson, S.; Armes, S. P. Synthesis of Surface-initiated Polymer Brushes using Macro-initiators. *Polym. Int.* **2009**, *58*, 307−316.

(42) Paik, M. Y.; Xu, Y.; Rastogi, A.; Tanaka, M.; Yi, Y.; Ober, C. K. Patterning of Polymer Brushes. A Direct Approach to Complex, Sub-surface Structures. *Nano Lett.* **2010**, *10*, 3873−3879.

(43) Rastogi, A.; Paik, M. Y.; Tanaka, M.; Ober, C. K. Direct Patterning of Intrinsically Electron Beam Sensitive Polymer Brushes. *ACS Nano* **2010**, *4*, 771−780.

(44) Mandal, K.; Balland, M.; Bureau, L. Thermoresponsive Micropatterned Substrates for Single Cell Studies. *PLoS One* **2012**, *7*, 1−7.

(45) Arumugam, S.; Orski, S. V.; Locklin, J.; Popik, V. V. Photoreactive Polymer Brushes for High-density Patterned Surface Derivatization using a Diels-Alder Photoclick Reaction. *J. Am. Chem. Soc.* **2012**, *134*, 179−182.

(46) Iwata, R.; Suk-In, P.; Hoven, V. P.; Takahara, A.; Akiyoshi, K.; Iwasaki, Y. Control of Nanobiointerfaces Generated from Well-defined Biomimetic Polymer Brushes for Protein and Cell Manipulations. *Biomacromolecules* **2004**, *5*, 2308−2314.

(47) Panzarasa, G.; Soliveri, G.; Sparnacci, K.; Ardizzone, S. Patterning of Polymer Brushes Made Easy using Titanium Dioxide: Direct and Remote Photocatalytic Lithography. *Chem. Commun.* **2015**, *51*, 7313−7316.

(48) Ahmad, S. A.; Leggett, G. J.; Hucknall, A.; Chilkoti, A. Micro-and Nanostructured Poly[oligo(ethylene glycol)methacrylate] Brushes Grown from Photopatterned Halogen Initiators by Atom Transfer Radical Polymerization. *Biointerphases* **2011**, *6*, 8−15.

(49) Ahn, S. J.; Kaholek, M.; Lee, W.-K.; LaMattina, B.; LaBean, T. H.; Zauscher, S. Surface-Initiated Polymerization on Nanopatterns Fabricated by Electron-Beam Lithography. *Adv. Mater.* **2004**, *16*, 2141−2145.

(50) Okazaki, S. High Resolution Optical Lithography or High Throughput Electron Beam Lithography: The Technical Struggle from the Micro to the Nano-fabrication Evolution. *Microelectron. Eng.* **2015**, *133*, 23−35.

(51) Hu, Z.; Shao, Q.; Moloney, M. G.; Xu, X.; Zhang, D.; Li, J.; Zhang, C.; Huang, Y. Nondestructive Functionalization of Graphene by Surface-Initiated Atom Transfer Radical Polymerization: An Ideal Nanofiller for Poly(p-phenylene benzobisoxazole) Fibers. *Macromolecules* **2017**, *50*, 1422−1429.

(52) Rajender, N.; Suresh, K. I. Surface-Initiated Atom Transfer Radical Polymerization (SI-ATRP) From Graphene Oxide: Effect of Functionalized Graphene Sheet (FGS) on the Synthesis and Material Properties of PMMA Nanocomposites. *Macromol. Mater. Eng.* **2016**, *301*, 81−92.

(53) Yameen, B.; Khan, H. U.; Knoll, W.; Förch, R.; Jonas, U. Surface Initiated Polymerization on Pulsed Plasma Deposited Polyallylamine: A Polymer Substrate-independent Strategy to Soft Surfaces with Polymer Brushes. *Macromol. Rapid Commun.* **2011**, *32*, 1735−1740.

(54) Rodriguez-Emmenegger, C.; Kylián, O.; Houska, M.; Brynda, E.; Artemenko, A.; Kousal, J.; Alles, A. B.; Biederman, H. Substrate-independent Approach for the Generation of Functional Protein Resistant Surfaces. *Biomacromolecules* **2011**, *12*, 1058−1066.

(55) Wang, X.; Zhou, M.; Zhu, Y.; Miao, J.; Mao, C.; Shen, J. Preparation of a NovelImmunosensor for Tumor Biomarker Detection based on ATRP Technique. *J. Mater. Chem. B* **2013**, *1*, 2132−2138.

(56) Nandivada, H.; Chen, H. Y.; Lahann, J. Vapor-Based Synthesis of Poly[(4-formyl-p-xylylene)-co-(p-xylylene)] and Its Use for Biomimetic Surface Modifications. *Macromol. Rapid Commun.* **2005**, *26*, 1794−1799.

(57) Koenig, M.; Lahann, J. Nanotopographical Control of Surfaces using Chemical Vapor Deposition Processes. *Beilstein J. Nanotechnol.* **2017**, *8*, 1250−1256.

(58) Nandivada, H.; Chen, H. Y.; Bondarenko, L.; Lahann, J. Reactive Polymer Coatings that "Click. *Angew. Chem., Int. Ed.* **2006**, *45*, 3360−3363.

(59) Deng, X.; Friedmann, C.; Lahann, J. Bio-orthogonal "Double-Click" Chemistry Based on Multifunctional Coatings. *Angew. Chem., Int. Ed.* **2011**, *50*, 6522−6526.

(60) Chen, H.-Y.; Rouillard, J.-M.; Gulari, E.; Lahann, J. Colloids with High-definition Surface Structures. *Proc. Natl. Acad. Sci. U. S. A.* **2007**, *104*, 11173−11178.

(61) Jiang, X.; Chen, H.-Y.; Galvan, G.; Yoshida, M.; Lahann, J. Vapor-Based Initiator Coatings for Atom Transfer Radical Polymerization. *Adv. Funct. Mater.* **2008**, *18*, 27−35.

(62) Chen, H. Y.; Lahann, J. Vapor-assisted Micropatterning in Replica Structures: A Solventless Approach Towards Topologically and Chemically Designable Surfaces. *Adv. Mater.* **2007**, *19*, 3801−3808.

(63) Chen, H. Y.; Lahann, J. Designable Biointerfaces Using Vapor-based Reactive Polymers. *Langmuir* **2011**, *27*, 34−48.

(64) Teare, D. O. H.; Barwick, D. C.; Schofield, W. C. E.; Garrod, R. P.; Ward, L. J.; Badyal, J. P. S. Substrate-Independent Approach for Polymer Brush Growth by Surface Atom Transfer Radical Polymerization. *Langmuir* **2005**, *21*, 11425−11430.

(65) Coad, B. R.; Styan, K. E.; Meagher, L. One Step ATRP Initiator Immobilization on Surfaces Leading to Gradient-Grafted Polymer Brushes. *ACS Appl. Mater. Interfaces* **2014**, *6*, 7782−7789.

(66) Shi, Y.; Menzies, D. J.; Tsang, K. M.; Del Borgo, M. P.; Easton, C. D.; Aguilar, M.-I.; Perlmutter, P.; Truong, V. X.; Forsythe, J. S. A Versatile and Rapid Coating Method via a Combination of Plasma Polymerization and Surface-initiated SET-LRP for the Fabrication of Low-fouling Surfaces. *J. Polym. Sci., Part A: Polym. Chem.* **2017**, *55*, 2527−2536.

(67) Saboohi, S.; Coad, B. R.; Michelmore, A.; Short, R. D.; Griesser, H. J. Hyperthermal Intact Molecular Ions Play Key Role in Retention of ATRP Surface Initiation Capability of Plasma Polymer

Films from Ethyl -Bromoisobutyrate. *ACS Appl. Mater. Interfaces* **2016**, *8*, 16493−1650216502.

(68) Madsen, J.; Ducker, R. E.; Al Jaf, O.; Cartron, M. L.; Alswieleh, A. M.; Smith, C. H.; Hunter, C. N.; Armes, S. P.; Leggett, G. J. Fabrication of Microstructured Binary Polymer Brush "Corrals" with Integral pH Sensing for Studies of Proton Transport in Model Membrane Systems. *Chem. Sci.* **2018**, *9*, 2238−2251.

(69) Crespo-Quesada, M.; Andanson, J. M.; Yarulin, A.; Lim, B.; Xia, Y.; Kiwi-Minsker, L. UV-ozone Cleaning of Supported Poly-(vinylpyrrolidone)-stabilized Palladium Nanocubes: Effect of Stabilizer Removal on Morphology and Catalytic Behavior. *Langmuir* **2011**, *27*, 7909−7916.

(70) Aliaga, C.; Park, J. Y.; Yamada, Y.; Lee, H. S.; Tsung, C.-k.; Yang, P.; Somorjai, G. A. Capping Agents from Pt Nanoparticles by UV - Ozone Treatment. *J. Phys. Chem. C* **2009**, *113*, 6150−6155.

(71) Sheridan, R. J.; Orski, S. V.; Muramoto, S.; Stafford, C. M.; Beers, K. L. Ultraviolet/Ozone as a Tool To Control Grafting Density in Surface-Initiated Controlled-Radical Polymerizations via Ablation of Bromine. *Langmuir* **2016**, *32*, 8071−8076.

(72) Ausserré, D.; Valignat, M.-P. Surface Enhanced Ellipsometric Contrast (SEEC) Basic theory and $\lambda/4$ Multilayered Solutions. *Opt. Express* **2007**, *15*, 8329−8339.

(73) Chen, Q.; Kooij, E.; Sui, X.; Padberg, C. J.; Hempenius, M. A.; Schön, P.; Vancso, G. *Soft Matter* **2014**, *10*, 3134−3142.

(74) Goda, T.; Ishihara, K.; Miyahara, Y. Critical Update on 2-methacryloyloxyethyl phosphorylcholine (MPC) Polymer Science. *J. Appl. Polym. Sci.* **2015**, *132*, 1.

(75) Wiarachai, O.; Vilaivan, T.; Iwasaki, Y.; Hoven, V. P. Clickable and Antifouling Platform of Poly[(propargyl methacrylate)-ran-(2-methacryloyloxyethyl phosphorylcholine)] for Biosensing Applications. *Langmuir* **2016**, *32*, 1184−1194.

(76) Zhang, Z.; Chen, S.; Chang, Y.; Jiang, S. Surface Grafted Sulfobetaine Polymers via Atom Transfer Radical Polymerization as Superlow Fouling Coatings. *J. Phys. Chem. B* **2006**, *110*, 10799−10804.